The cooling performance of a building integrated evaporative cooling system driven by solar energy

Miyazaki, Takahiko
Tokyo University of Agriculture and Technology, Institute of Engineering

Akisawa, Atsushi
Tokyo University of Agriculture and Technology, Institute of Engineering

Nikai, Isao
Engineering Consultant

出版情報：Energy and Buildings. 43 (9), pp.2211-2218, 2011-09. Elsevier
バージョン：

The cooling performance of a building integrated evaporative cooling system driven by solar energy

Takahiko Miyazaki[a,*], Atsushi Akisawa[a], Isao Nikai[b]

[a] *Tokyo University of Agriculture and Technology, Institute of Engineering, 2-24-16 Nakacho, Koganei, Tokyo 184-8588, Japan*
[b] *Engineering Consultant, 5-7-12 Kiminomori-minami, Ooami-shirasatomachi, Sanbugun, Chiba 299-3241, Japan*

Abstract

The solar chimney is a passive cooling technique to enhance the natural ventilation of buildings. The effect is, however, limited under hot and humid climatic conditions. In the study, the solar chimney was accompanied by a dew-point evaporative cooler. The dew-point evaporative cooler was integrated with the ceiling of a building. The air flow induced by the solar chimney was predicted by simulation, and the cooling effect of the dew-point evaporative cooler was also analyzed by heat and mass transfer simulation. The results showed that the system was capable of coping with internal heat gains of an ordinary office building. In addition, the optimal geometry of the evaporative cooling channel was revealed.

Keywords: Solar energy, Solar chimney, Maisotsenko cycle, Evaporative cooler

*Corresponding author
Email address: miyazaki@phase.cm.kyushu-u.ac.jp (Takahiko Miyazaki)
Current affiliation: Kyushu University, Faculty of Engineering Sciences, 6-1 Kasuga Koen, Kasuga-shi, Fukuoka 816-8580, Japan

1. Introduction

Buildings are large energy consumers in urban areas. In Japanese case, for instance, approximately one third of primary energy is consumed by residential and commercial buildings [1]. The heating of space is dominant for energy consumption in residential buildings because the traditional Japanese houses are made of wood, and kerosene or gas heaters are used in those houses. On the other hand, the cooling demand is dominant in commercial buildings, especially in office buildings, because of high-insulated and air-tight construction as well as increased office automation equipment. In the context of energy and environmental conservation, the solar heating/cooling is one of the most desirable schemes, one of technological challenges of which is the passive cooling technique in hot and humid climate.

The passive cooling can be defined as the cooling method without active mechanical devices such as pumps and fans, and the provision of cooling relies mainly on the air flow caused by the buoyancy[2]. Solar chimney, Trombe walls, and double facades are devices to induce the air flow by the stack effect, and the enhanced natural ventilation by those devices will deliver the cooling effect [3, 4, 5, 6, 7]. The natural ventilation may, however, harm the thermal comfort of buildings if it is implemented in hot and humid climate because the temperature and humidity of outdoor air are much higher than those of the air-conditioned room during daytime. Even at night, it is not rare in Japan that the outdoor air temperature exceeds 25°C throughout the night during the summer season.

One way to cool the outdoor air before it is supplied to the space is the evaporative cooling. The evaporative cooling technique can be used either

with active systems or with passive systems. The studies of evaporative cooling for passive systems are not many, however, and the technology to integrate it with building structure is still under development [2]. Raman et al. [8] tested passive solar systems, which provided heating, cooling and ventilation, in composite climate including hot-dry, hot-humid and cold climate. It was presented that the passive system, which consisted of a south wall collector and a roof duct with evaporative cooling surface, moderated the temperature variation of the room, and the room temperature was kept around 30°C when the ambient temperature was 42°C at maximum during the summer period. Chungloo and Limmeechokchai [9] conducted performance measurement of a solar chimney combined with a water sprayed roof. The results showed that the combination of the two passive measures decreased the room air temperature by 2.0–6.2°C compared with the ambient temperature. Maerefat and Haghighi [10] investigated a system with a solar chimney and an evaporative cooling cavity by using a mathematical model. The effects of the geometrical dimensions as well as of the ambient conditions on the cooling performance were analyzed, and the results showed that the proposed system was capable of improving the indoor conditions even with low solar intensity of 200W/m^2 and high ambient temperature of 40°C. The room air temperature strongly depended on the relative humidity of the ambient air, however. They concluded that the system provided comfortable indoor air conditions at high ambient temperature with the relative humidity lower than 50%.

The purpose of the study is to develop a passive cooling device that will effectively reduce the cooling load of main air conditioners under hot

and humid climatic conditions. The authors have proposed the building integration of a passive cooling system that consisted of a solar chimney and a dew point evaporative cooler [11]. This article reports the simulation of the cooling performance of the system with a modified design.

2. The system description

2.1. The building integrated solar cooling system

Our attempt is the integration of the solar cooling system into architecture. Fig. 1 depicts an overview of the building integrated evaporative cooling system and the direction of the air movement. The building is featured with a solar chimney that is attached to the south-facing wall. The evaporative cooler is integrated with the ceiling panel so that the wet channel is adjacent to the room side. The evaporative cooler is called the M-Cycle [12]. In our previous design, the dry channel of the M-Cycle was adjacent to the room to avoid problems that may arise from water leakage and penetration. The design was, however, inferior to the present design in the cooling effect.

The air inside the solar chimney is heated by the solar radiation, and the upward flow is generated due to the stack effect. The upward flow inside the chimney induces the air movement in the room. By connecting the air exit of the evaporative cooler with the inlet of the solar chimney, the air travels through the evaporative cooler before it flows the solar chimney. The inlet air duct of the evaporative cooler can be connected either to the room or to the outdoor. In hot humid climate, the inlet air of the evaporative cooler should be the conditioned room air so that the temperature of the ceiling panel is lower than the room air temperature. In this case, the cooling effect

is owing to the dehumidified air by the room air conditioner, and the system assists the room air conditioner by reducing the cooling load. If the outdoor air is moderate in terms of temperature and humidity, the inlet air to the evaporative cooler can be the outdoor air. The system will provide cooling without any dehumidification work.

2.2. The dew point evaporative cooler

The evaporative cooler is a device to lower the air temperature by the latent heat of water. The water as a refrigerant evaporates by taking heat from the working air, and hence the working air is cooled and humidified. The working air has a potential to contain the moisture to saturation, which limits the cooled temperature of the working air to its wet-bulb temperature. The dew point evaporative cooler that works based on the principle of the Maisotsenko cycle (the M-Cycle) [12] overcame the cooling limit, and the incoming air can be cooled to its dew point temperature theoretically.

The basic structure of the M-Cycle evaporative cooler and the temperature and humidity ratio variations are illustrated in Fig. 2. Two air flow channels are adjoining and the wall of one of the channels is covered with fabric or water absorbing sheet so that the wall is wet. The air first flows the dry channel from 1 to 2 and then it is redirected to the wet channel. Water in the wet channel is heated by the air in the dry channel and evaporates on the surface of the wet wall. Because of the counter flow, the air in the dry channel is cooled through 1 to 2, while the temperature of the air in the wet channel increases from 2 to 3. Because the wet bulb temperature of the air decreases through the dry channel from 1 to 2, air temperature finally reaches the dew point at the point 2.

Without any heat input to the M-Cycle, the temperature at the exit of the wet channel (state 3) is the wet bulb of the state 1. The enthalpy is balanced between the dry channel and the wet channel as shown in Eq.(1).

$$\dot{m}_a (h_1 - h_2) = \dot{m}_a (h_3 - h_2) \tag{1}$$

In this case, no work is extracted from the M-Cycle. To produce cooling effect for the outer system, either a part of the cooled air is extracted at the state 2, or heat load is given to the refrigerant in the wet channel from outside. The proposed system uses the latter configuration. When the water in the wet channel receives heat not only from the dry channel but also from other heat sources such as room air, the enthalpy change in the wet channel has to be extended, and the exit condition moves on the saturation line toward a higher temperature and a larger humidity ratio. The temperature at the exit of the wet channel can be a few degrees lower than that at the inlet of the dry channel, and therefore the air condition at the exit of the wet channel changes from the state 3 to the state 3' as shown in Fig. 2.

The heat balance with the additional heat input would be expressed by Eq.(2) or by the form of Eq.(3).

$$\dot{m}_a (h_1 - h_2) + \dot{Q} = \dot{m}_a (h_3' - h_2) \tag{2}$$

$$\dot{Q} = \dot{m}_a (h_3' - h_3) \tag{3}$$

where, Q is the additional heat input to the M-Cycle and it is equivalent to the maximum cooling capacity of the ceiling integrated evaporative cooling system.

The water consumed in the wet channel has to be complemented by water supply. Similarly to humidifiers, water treatment will be necessary to remove minerals and pollutants, and it will cause an increase in installation cost. On the other hand, the running cost with respect to water consumption will be negligible because the quantity of the water consumption is much smaller than that of air flow rate. For instance, the humidity ratio change in the wet channel will be less than 10 g/kg in the case shown in Fig. 2.

3. The simulation models

The performance of the solar chimney driven evaporative cooler was predicted by two steps. At first, the air flow induced by the solar chimney was predicted by simulation. The simulation model followed the mathematical model proposed by Ong [13]. The authors have compared the mathematical model with the computational fluid dynamics (CFD) model in terms of the air flow rate and the chimney outlet temperature [14]. The air gap width of the chimney was set to 0.3 m in the CFD model, and the results showed that the difference in the air flow rate was less than 5% between the mathematical model and the CFD model. It was also shown that the predicted outlet temperature was reasonably close between the two models. Then, the temperature profiles of the evaporative coolers were calculated by solving the governing equations of heat and mass transfer.

3.1. The mathematical model of the solar chimney

The solar chimney consisted of the outer glass layer and the inner wall layer, and the air flow would be generated in the gap between the layers. It was assumed that the room side of the wall was well-insulated and the heat

flux through the wall to the room was negligible. The solar chimney model is illustrated in Fig. 3. The heat balances with respect to the glass, the air inside the chimney, and the wall were expressed as Eqs.(4)–(6).

$$S_{\mathrm{g}} + \alpha_{\mathrm{g}}(T_{\mathrm{f}} - T_{\mathrm{g}}) + \beta_{\mathrm{gw}}(T_{\mathrm{w}} - T_{\mathrm{g}}) + (\alpha_{\mathrm{wind}} + \beta_{\mathrm{gs}})(T_{\mathrm{a}} - T_{\mathrm{g}}) = 0 \tag{4}$$

$$\dot{q}_{\mathrm{f}} = \alpha_{\mathrm{g}}(T_{\mathrm{g}} - T_{\mathrm{f}}) + \alpha_{\mathrm{w}}(T_{\mathrm{w}} - T_{\mathrm{f}}) \tag{5}$$

$$S_{\mathrm{w}} + \alpha_{\mathrm{w}}(T_{\mathrm{f}} - T_{\mathrm{w}}) + \beta_{\mathrm{gw}}(T_{\mathrm{g}} - T_{\mathrm{w}}) = 0 \tag{6}$$

The convective heat transfer coefficients, α_{g} and α_{w}, were found by the empirical correlations for the free convection flow on the vertical plane, which is given in Eq.(7) [15].

$$Nu = \begin{cases} \left\{0.825 + 0.387Ra^{1/6} / \left[1 + (0.492/Pr)^{9/16}\right]^{8/27}\right\}^2 & (Ra > 10^9) \\ 0.68 + 0.670Ra^{1/4} / \left[1 + (0.492/Pr)^{9/16}\right]^{4/9} & (Ra \leq 10^9) \end{cases} \tag{7}$$

On the other hand, the heat transfer coefficient by wind, α_{wind} was given as a function of the wind velocity, u_{wind}, by Eq.(8) [16].

$$\alpha_{\mathrm{wind}} = 10.21u_{\mathrm{wind}} + 4.47. \tag{8}$$

The radiative heat transfer coefficients, β_{gw} and β_{gs}, were defined as follows:

$$\beta_{\mathrm{gw}} = \frac{\sigma(T_{\mathrm{g}} + T_{\mathrm{w}})(T_{\mathrm{g}}^2 + T_{\mathrm{w}}^2)}{1/\epsilon_{\mathrm{g}} + 1/\epsilon_{\mathrm{w}} - 1} \tag{9}$$

$$\beta_{\mathrm{gs}} = \sigma\epsilon_{\mathrm{g}}(T_{\mathrm{s}} + T_{\mathrm{g}})(T_{\mathrm{s}}^2 + T_{\mathrm{g}}^2)\frac{(T_{\mathrm{s}} - T_{\mathrm{g}})}{(T_{\mathrm{a}} - T_{\mathrm{g}})} \tag{10}$$

T_{s} is the sky temperature, which is calculated by Eq.(11) [17].

$$T_{\mathrm{s}} = T_{\mathrm{a}} \left[0.711 + 0.0056 t_{\mathrm{dp}} + 0.000073 t_{\mathrm{dp}}^2 + 0.013 \cos(15 hr)\right]^{1/4} \tag{11}$$

where, t_{dp} represents the dew point temperature of the outdoor air in degree Celsius, and hr denotes the hour from midnight.

$\dot{q}_{\mathrm{f}}$ in Eq.(5) represents the heat flux to the fluid, which is given by the following expression.

$$\dot{q}_{\mathrm{f}} = \frac{\rho_{\mathrm{a}} c_{p\mathrm{a}} \dot{V}_{\mathrm{f}}}{WH} (T_{\mathrm{f,o}} - T_{\mathrm{f,i}}) \tag{12}$$

where, W denotes the chimney width, and H denotes the chimney height.

$T_{\mathrm{f,i}}$ and $T_{\mathrm{f,o}}$ are the temperatures of the fluid at the inlet and at the outlet of the chimney, respectively, and the mean fluid temperature can be estimated by Eq.(13).

$$T_{\mathrm{f}} = \gamma T_{\mathrm{f,o}} + (1 - \gamma) T_{\mathrm{f,i}} \tag{13}$$

The value of γ will vary depending on the shape of the chimney because the bulk mean temperature changes in accordance with the temperature, density and velocity distributions. We found that $\gamma = 0.5$ was a good approximation to represent the mean fluid temperature under our configuration of the solar chimney based on the CFD analysis [14].

By substituting Eq.(13) for Eq.(12), we obtain Eq.(14).

$$\dot{q}_{\mathrm{f}} = \frac{\rho_{\mathrm{a}} c_{p\mathrm{a}} \dot{V}_{\mathrm{f}}}{\gamma WH} (T_{\mathrm{f}} - T_{\mathrm{f,i}}) \tag{14}$$

The formula to predict the air flow rate due to buoyancy was presented by Andersen [18]. The air flow rate could be expressed based on the temperature difference between the fluid and the ambient as Eq.(15).

$$\dot{V}_{\mathrm{f}} = C_{d\mathrm{i}} A_{\mathrm{i}} \left(\frac{2gH_{\mathrm{i}}\Delta T}{T_{\mathrm{f}}} \right)^{1/2} \tag{15}$$

where, A_{i} is the inlet aperture area, and $C_{d\mathrm{i}}$ is the discharge coefficient at the inlet. H_{i} is the hight from the center of the inlet aperture to the neutral pressure plane.

3.2. The mathematical model of the M-Cycle

The temperature profiles of the air in the M-Cycle and the ceiling surface were predicted by the mathematical model. The model was based on the heat and mass balances of a small control volume, which is illustrated in Fig. 4. The model used the following assumptions:

- The enthalpy balance of the wet air can be expressed independently by the sensible heat balance and by the mass balance (latent heat balance).
- The water absorbing sheet can maintain water on the surfaces of heat transfer plate and of the ceiling, and the air is in saturation at the interface between the water absorbing sheet layer and the air layer.
- The effects of the conductive heat transfer in horizontal direction inside the heat transfer plate, the water absorbing sheet, and the ceiling are negligible.
- The upper side of the dry channel is well insulated so that the heat gain through the roof is minimal.

The sensible heat balances of the air in the dry channel and in the wet channel were expressed by Eqs.(16) and (17).

$$\rho_{\mathrm{d}} c_{p\mathrm{d}} u_{\mathrm{d}} a_{\mathrm{d}} \frac{\mathrm{d}T_{\mathrm{d}}}{\mathrm{d}z} = \alpha_{\mathrm{d}} \left(T_{\mathrm{p}} - T_{\mathrm{d}}\right) \tag{16}$$

$$\rho_{\mathrm{w}} c_{p\mathrm{w}} u_{\mathrm{w}} a_{\mathrm{w}} \frac{\mathrm{d}T_{\mathrm{w}}}{\mathrm{d}z} = \alpha_{\mathrm{w1}} \left(T_{\mathrm{s1}} - T_{\mathrm{w}}\right) + \alpha_{\mathrm{w2}} \left(T_{\mathrm{s2}} - T_{\mathrm{w}}\right) \tag{17}$$

The subscripts d, w, and s represent the dry channel, the wet channel, and the water absorbing sheet, respectively, and w1 and w2 represent the heat transfer plate side (upper side) of the wet channel and the ceiling side (lower side) of the wet channel, respectively. The subscripts s1 and s2 are in a similar definition.

The mass balance of the wet channel was expressed by Eq.(18).

$$\rho_{\mathrm{DA}} u_{\mathrm{w}} a_{\mathrm{w}} \frac{\mathrm{d}X_{\mathrm{w}}}{\mathrm{d}z} = \rho_{\mathrm{DA}} \left(\alpha_{\mathrm{m1}} + \alpha_{\mathrm{m2}}\right) \left(X_{\mathrm{w}}^{*} - X_{\mathrm{w}}\right) \tag{18}$$

where, X_{w}^{*} denotes the humidity ratio of the saturated air at temperature T_{w}.

The energy balances concerning the heat transfer plate, the water absorbing sheets, and the ceiling were expressed by Eqs.(19)–(22), respectively.

$$\alpha_{\mathrm{d}} \left(T_{\mathrm{d}} - T_{\mathrm{p}}\right) + \frac{k_{\mathrm{e1}}}{a_{\mathrm{e2}}} \left(T_{\mathrm{s1}} - T_{\mathrm{p}}\right) = 0 \tag{19}$$

$$\frac{k_{\mathrm{e1}}}{a_{\mathrm{e1}}} \left(T_{\mathrm{p}} - T_{\mathrm{s1}}\right) + \alpha_{\mathrm{w1}} \left(T_{\mathrm{w}} - T_{\mathrm{s1}}\right) + \rho_{\mathrm{DA}} \alpha_{\mathrm{m1}} r \left(X_{\mathrm{w}} - X_{\mathrm{w}}^{*}\right) = 0 \tag{20}$$

$$\frac{k_{\mathrm{e2}}}{a_{\mathrm{e2}}} \left(T_{\mathrm{c}} - T_{\mathrm{s2}}\right) + \alpha_{\mathrm{w2}} \left(T_{\mathrm{w}} - T_{\mathrm{s2}}\right) + \rho_{\mathrm{DA}} \alpha_{\mathrm{m2}} r \left(X_{\mathrm{w}} - X_{\mathrm{w}}^{*}\right) = 0 \tag{21}$$

$$\frac{k_{\mathrm{e2}}}{a_{\mathrm{e2}}} \left(T_{\mathrm{s2}} - T_{\mathrm{c}}\right) + \alpha_{\mathrm{r}} \left(T_{\mathrm{r}} - T_{\mathrm{c}}\right) + \dot{q}_{R} = 0 \tag{22}$$

where, a_{e1} and a_{e2} are effective thickness of the heat transfer plate and that of the ceiling, respectively, and they are defined as $a_{e1} = a_p + a_{s1}$ and $a_{e2} = a_c + a_{s2}$, respectively. k_{e1} and k_{e2} are the effective thermal conductivity of the heat transfer plate and that of the ceiling and they are defined as $k_{e1} = a_{e1}/(a_p/k_p + a_{s1}/k_{s1})$ and $k_{e2} = a_{e2}/(a_c/k_c + a_{s2}/k_{s2})$, respectively. α_d, α_{w1} and α_{w2} are the heat transfer coefficients between the air and the wall surfaces in the dry and wet channels. α_r is the heat transfer coefficient between the room air and the ceiling surface, and given by $\alpha_r = 1.52(\Delta T)^{0.33}$ [19]. The heat input to the ceiling by radiative heat exchange is given by $\dot{q}_R$.

The heat transfer coefficients inside the dry and wet channels were approximated by the Nusselt number of the developed laminar flow in rectangular shape channels under the condition of uniform heat flux along the flow direction and the uniform wall temperature at a cross section. The three side walls of the dry channel were insulated, while the two side walls facing each other were insulated in case of the wet channel. Thus, the Nusselt numbers were 5.38 and 8.23 for the dry channel and for the wet channel, respectively [20]. The effect of the entrance region was ignored because the heat transfer coefficient at the entrance region was higher than that of the fully developed region. Therefore, the performance would not be over-estimated due to the neglect of the entrance region. To find the mass transfer coefficient inside the wet channel, a simple assumption where the Lewis number equals one was used. Then, the mass transfer coefficient was given as $\alpha_m = \alpha_w/(\rho_w c_{pw})$.

3.3. The integration of the solar chimney and the evaporative cooler

The air flow rate of the solar chimney expressed by Eq.(15) was derived from the pressure difference between the inside and the outside at the inlet

of the solar chimney. In the case of the M-Cycle integrated solar chimney, the dry and wet channels of the M-Cycle will cause a large resistance to the air flow of the solar chimney. Because the pressure drop by the M-Cycle would be dominant for the air flow rate, the air flow rate induced by the solar chimney was estimated by taking into account the pressure drop from the inlet of the M-Cycle to inside the solar chimney.

The pressure drop due to the M-Cycle was expressed by Eq.(23).

$$\Delta P_{\mathrm{M}} = \frac{1}{2}\rho_{\mathrm{a}}\zeta_{\mathrm{M,i}}u'^{2}_{\mathrm{Mi}} + \frac{1}{2}\rho_{\mathrm{a}}\left(\lambda_{\mathrm{M}}\frac{2L}{d_{\mathrm{M}}} + \zeta_{\mathrm{rev}} + \zeta_{\mathrm{C,i}}\right)u^{2}_{\mathrm{M}} \tag{23}$$

where, u'_{Mi} and u_{M} denote the velocity of vena contracta at the inlet of the M-Cycle and the velocity of the air inside the M-Cycle, respectively. The friction coefficient is given by λ_{M} and the loss coefficients at the inlet of the M-Cycle, at the reverse section and at the inlet to the solar chimney (the exit of the M-Cycle) are represented by $\zeta_{\mathrm{M,i}}$, ζ_{rev} and $\zeta_{\mathrm{C,i}}$, respectively. L is the length of the channel, and d_{M} is the hydraulic diameter of the channel.

Then, the pressure difference between the inlet of the M-Cycle (P_{r}) and the inside of the solar chimney (P_{Ci}) could be given by:

$$\Delta P_{\mathrm{i}} = P_{\mathrm{r}} - P_{\mathrm{Ci}} = \frac{1}{2}\rho_{\mathrm{a}}u'^{2}_{\mathrm{Ci}} + \Delta P_{\mathrm{M}} \tag{24}$$

Using the mass balance, $\rho_{\mathrm{a}}C_{c\mathrm{M,i}}A_{\mathrm{M,i}}u'_{\mathrm{M,i}} = \rho_{\mathrm{a}}A_{\mathrm{M}}u_{\mathrm{M}} = \rho_{\mathrm{a}}C_{c\mathrm{C,i}}A_{\mathrm{C,i}}u'_{\mathrm{C,i}}$, Eq.(24) could be rewritten as Eq.(25).

$$\Delta P_{i} = \frac{1}{2}\rho_{\mathrm{a}}\psi u'^{2}_{\mathrm{M,i}} \tag{25}$$

where, ψ was defined by Eq.(26).

$$\psi = \left(\frac{C_{c\mathrm{M,i}} A_{\mathrm{M,i}}}{C_{c\mathrm{C,i}} A_{\mathrm{C,i}}}\right)^2 + \zeta_{\mathrm{M,i}} + \left(\lambda_{\mathrm{M}} \frac{2L}{d_{\mathrm{M}}} + \zeta_{rev} + \zeta_{C,i}\right) \left(\frac{C_{c\mathrm{M,i}} A_{\mathrm{M,i}}}{A_{\mathrm{M}}}\right)^2 \quad (26)$$

where, $C_{c\mathrm{C,i}}$ and $C_{c\mathrm{M,i}}$ are the contraction coefficients at the inlet of the M-Cycle and at the inlet of the solar chimney, respectively. $A_{\mathrm{C,i}}$ denotes the inlet aperture area of the solar chimney. $A_{\mathrm{M,i}}$ and A_{M} represent the inlet aperture area and the sectional area of the M-Cycle, respectively.

Similar to the case of a single solar chimney, the air flow rate could be predicted by Eq.(27).

$$V_{\mathrm{M}} = C_{d\mathrm{M}} A_{\mathrm{M,i}} \sqrt{\frac{2\Delta T g H_{\mathrm{M}}}{\overline{T}_{\mathrm{f}}}} \quad (27)$$

where, $C_{d\mathrm{M}}$ is the discharge coefficient including the M-Cycle, and it is defined as $C_{d\mathrm{M}} = C_{c\mathrm{M,i}}/\sqrt{\psi}$.

3.4. The cooling performance of the system

The system provides radiative cooling by direct heat exchange between the ceiling surface and the objects in the room such as people, furniture and appliances. The radiative cooling effect was expressed by $\dot{q}_R$ in the model. On the other hand, the convective heat transfer between the ceiling surface and the room air results in the convective cooling effect. The convective cooling effect at local position was defined as $\dot{q}'_C = \alpha_{\mathrm{r}} (T_{\mathrm{r}} - T_{\mathrm{c}})$. Then, the global average of the convective cooling effect was defined by:

$$\dot{q}_C = \int_0^L \dot{q}'_C \mathrm{d}z / L \quad (28)$$

4. Results and discussion

4.1. The conditions of the simulation

The weather data were taken from a reference [21]. The outdoor air temperature and the humidity ratio are shown in Fig. 5, and the solar radiation on the horizontal and vertical surfaces are given in Fig. 6. A constant wind velocity of 1 m/s was used for the simulation of the solar chimney.

The simulations of the solar chimney and the M-Cycle were based on the conditions as follows.

The solar chimney. The chimney was consisted of the outer glass layer and the inner wall layer. The radiation properties of the materials are given in Table 1. The geometry of the solar chimney was 3 m in height, 1 m in width. It was assumed that the air gap in the chimney was 0.3 m, which was near the optimum to maximized the air flow rate [14]. The inlet and outlet apertures were the same size and it was 0.1 m $\times$ 1 m. The contraction coefficient was assumed as 0.6 for both apertures. The value of γ in Eq.(13) was 0.5.

The M-Cycle. The length of the channel was 5 m and the width was 1 m. The gap width of both the air flow channels was 25 mm under a nominal standard condition. The value was changed for parametric analysis. The aperture size was 0.1 m $\times$ 1 m for both the inlet and outlet apertures. The material, thickness and thermal conductivity of the heat transfer plate, the water absorbing sheet and the ceiling are given in Table 2. The inlet air to the M-Cycle was the conditioned room air. It was assumed that the temperature and the relative humidity of the room were maintained at 26 °C and 50%, respectively, by a room air-conditioner.

4.2. The airflow induced by the solar chimney

The hourly variations of the air flow induced by the solar chimney are shown in Fig. 7. The effect of the channel width of the M-Cycle on the air flow rate was also presented in the figure. The results showed that the sufficient air flow could be obtained when solar radiation was available.

The channel width of the M-Cycle was influential on the air flow rate. The air flow rate was amplified by the wider channel width because the pressure drop was mitigated. On the other hand, the wider channel width will result in a lower cooling performance because the heat transfer area per channel volume will decrease. As the system contributes to energy savings in terms of reductions of mechanical ventilation work as well as of air-conditioning load, the optimal geometry of the M-Cycle has to be chosen by the consideration of both the air flow rate and the cooling performance.

4.3. The temperature distribution on the cooled surface

The prediction of the M-Cycle performance was carried out under the condition where the air flow rate was 45 m^3/h . Fig. 8 shows the temperature profiles of the air and the ceiling for the case of no radiative cooling load and the radiative cooling load of 40 W/m^2.

At the M-Cycle part of the system, the air first enters the dry channel from the inlet located nearby the south wall, and flows toward the direction of interior of the room. The air flow direction is reversed at the end of the dry channel, and then the air flows back in the wet channel to the solar chimney attached to the south wall. It was shown that the air temperature was gradually decreased in the dry channel and it was the minimum at the farthest side. The ceiling temperature was also varied correspondingly.

The ceiling temperature should be lower than the room temperature to provide cooling effect, but it was strongly affected by the radiative cooling load $\dot{q}_R$. In the case of the no radiative cooling load, the ceiling temperature was under 22 °C throughout the surface. In the case of $\dot{q}_R = 40$ W/m^2, however, the ceiling temperature was close to the room temperature around the inlet of the M-Cycle. The results implied that 40 W/m^2 of the cooling load was close to the maximum cooling capacity of the system.

4.4. The cooling capacity of the system

The effects of the radiative cooling load on the convective cooling capacity and the average ceiling temperature are shown in Figs. 9 and 10. Fig. 9 was based on the constant air flow rate of 45 m^3/h with the variations of the channel width 15–30 mm. While, Fig. 10 was under the fixed channel width at 25 mm and the air flow rate was varied from 15 to 60 m^3/h.

The both results showed the decreasing convective cooling capacity and the increasing average ceiling temperature by the magnification of the radiative cooling load. The overall cooling capacity of the system was the sum of the radiative and convective cooling loads, and the overall cooling capacity was amplified with the increase of the radiative cooling load. The larger radiative cooling load would, however, have a negative effect on the thermal comfort of the room because of the higher ceiling temperature.

As a result, the overall cooling capacity of the system would depend on the internal conditions of the room, such as the heat emission from people and equipment as well as the temperature of them. Compared with internal heat gains from people and equipment, which would be around 50 W/m^2 for an ordinary office building, for example, it could be expected that the

proposed system was capable of removing those internal heat gains if all the ceiling surface was covered by the system. In addition, it was reported that the maximum cooling loads of existing office buildings in Japan were approximately 50–100W/m^2 [22]. Compared with these ranges of maximum cooling load, the cooling capacity of 50W/m^2 has a potential to cover 50%–100% of the maximum cooling load of an office building. Even if the proposed system is used for a quarter of the ceiling area, the system can reduce the maximum cooling load by more than 10%.

Another finding from the results was that the cooling effect could be enhanced by the narrower channel width, but the negative effect of reduced air flow rate was strong in the case of the low air flow rate. As it was shown in Fig. 7, the channel width was dominant for the air flow rate induced by the solar chimney. Even though the M-Cycle performance was improved by the narrow channel width, the cooling effect of the system would be diminished due to the low air flow rate.

4.5. The hourly cooling performance

The convective cooling capacity of the system was predicted based on the hourly air flow rate shown in Fig. 7. Fig. 11 depicts the hourly variation of the convective cooling capacity in the case of no radiative cooling load, while Fig. 12 depicts that with the radiative cooling load of 30 W/m^2.

When the radiative cooling load was not given to the system, the convective cooling capacity was the largest with the channel width of 20 mm during the daytime. While, the largest convective cooling capacity during the daytime was obtained by the channel width of 25 mm in the case of the radiative cooling load of 30 W/m^2. The difference would be due to the effect of the

enhanced air flow rate on the improvement of the cooling capacity. As shown in Fig. 10, the effect of the air flow rate on the convective cooling capacity was more significant when the radiative cooling load was larger. Therefore, the optimum channel width was extended with larger radiative cooling load.

Assuming that the system has to cope with some radiative cooling load, the optimum configuration of the system would be the channel width of 25 mm. Up to the channel width of 25 mm, the increase of the air flow rate was dominant for the improvement of the cooling capacity. By the further increment of the channel width, the positive effect of the increased air flow rate would be overwhelmed by the deterioration of the cooling effect due to the wider channel width.

5. Conclusions

The study proposed the solar chimney driven evaporative cooling system that was integrated with the ceiling of a room. The cooling performance of the system was predicted by simulation of the solar chimney and the M-Cycle evaporative cooling channel. The main findings of the study are summarized as follows.

- The proposed system was feasible as a solar energy driven cooling system because the sufficient air flow to the M-Cycle evaporative cooling channel could be induced by the solar chimney when the solar radiation was available.

- The system was capable of coping with the radiative cooling load as much as 40–50 W/m^2 without a severe increase of the ceiling temperature. It was expected that the internal heat gains of buildings could

be removed by the proposed system. Compared with the maximum cooling load of office buildings in Japan, it is expected that the system can reduce the maximum cooling load by more than 10% if a quarter of the ceiling area is replaced with the proposed system.

- The channel width of the M-Cycle was an influential parameter on the air flow rate of the solar chimney as well as the cooling effect of the M-Cycle. The optimum channel width to maximize the convective cooling capacity during the daytime would exist depending on the radiative cooling load, and it was 25 mm in the case of the radiative cooling load of 30 W/m^2. The further increase of the channel width would result in the deterioration of the cooling capacity because the negative effect of the wider channel width would overwhelm the effect of the increased air flow rate.

The paper presented a concept of solar chimney driven evaporative cooling system, and the performance of the system was predicted by simulation. The verifications of the solar-induced air flow rate and the cooling performance are necessary as a next step, which will be our future work.

Nomenclature

A area, m^2

a channel height, m

C_c contraction coefficient, –

C_d discharge coefficient, –

c_p specific heat, J kg^{-1} K^{-1}

d	hydraulic diameter, m
g	gravitational acceleration, m s^{-2}
H	height, m
h	enthalpy, J kg^{-1}
hr	hour from midnight, hour
k	thermal conductivity, W m^{-1} K^{-1}
L	length, m
$\dot{m}$	mass flow rate, kg s^{-1}
P	pressure, Pa
$\dot{Q}$	heat load, W
$\dot{q}$	heat flux, W m^{-2}
$\dot{q}_C$	convective cooling load, W m^{-2}
$\dot{q}_R$	radiative cooling load, W m^{-2}
r	latent heat of water, J kg^{-1}
S	solar radiation, W m^{-2}
T	temperature, K
t	temperature, °C
u	velocity, m s^{-1}
$\dot{V}$	volume flow rate, m^3 s^{-1}
W	width, m
X	humidity ratio, kg kg^{-1}
X^*	humidity ratio of saturated air, kg kg^{-1}

z position, m

Greek symbols

α convective heat transfer coefficient, W m^{-2} K^{-1}

α_m mass transfer coefficient, m s^{-1}

β radiative heat transfer coefficient, W m^{-2} K^{-1}

ϵ emissivity, –

λ friction loss coefficient, –

ρ density, kg m^{-3}

σ the Stefan-Boltzmann constant, W m^{-2} K^{-4}

ζ loss coefficient, –

Subscripts

a air or outdoor air

C solar chimney

c ceiling

DA dry air

d dry channel

dp dew point

f air in the solar chimney

g glass

i inlet

M the M-cycle

o outlet

p	heat transfer plate
r	room
rev	reverse section
s	sky
s1, s2	water absorbing sheet
w	wall or wet channel
wind	wind

References

[1] Agency for Natural Resources and Energy, Ministry of Economy, Trade and Industry, Energy in Japan, `http://www.enecho.meti.go.jp/english/`, Accessed 13/09/10.

[2] H.Y. Chan, S.B. Riffat, J. Zhu, Review of passive solar heating and cooling technologies, Renewable Sustainable Energy Rev. 14 (2010) 781–789.

[3] A. Bouchair, Solar chimney for promoting cooling ventilation in southern Algeria, Building Serv. Eng. Res. Technol. 15 (1994) 81–93.

[4] F. Flourentzou, J. Van der Maas, C.A. Roulet, Natural ventilation for passive cooling: measurement of discharge coefficients, Energy Build. 27 (1998) 283–292.

[5] M.M. AboulNaga, S.N. Abdrabboh, Improving night ventilation into low-rise buildings in hot-arid climates exploring a combined wall-roof solar chimney, Renewable Energy 19 (2000) 47–54.

[6] J. Khedari, N. Rachapradit, J. Hirunlabh, Field study of performance of solar chimney with air conditioned building, Energy 28 (2003) 1099–1114.

[7] E. Gratia, A. De Herde, Natural cooling strategies efficiency in an office building with a double-skin facade, Energy Build. 36 (2004) 1139–1152.

[8] P. Raman, S. Mande, V.V.N. Kishore, A passive solar system for thermal comfort conditioning of buildings in composite climate, Sol. Energy 70 (2001) 319–329.

[9] S. Chungloo, B. Limmeechokchai, Application of passive cooling systems in the hot and humid climate: The case study of solar chimney and wetted roof in Thailand, Build. Environ. 42 (2007) 3341–3351.

[10] M. Maerefat, A.P. Haghighi, Natural cooling of stand-alone houses using solar chimney and evaporative cooling cavity, Renewable Energy 35 (2010) 2040–2052.

[11] T. Miyazaki, A. Akisawa, I. Nikai, Study on the Maisotsenko cycle evaporative cooler driven by the solar chimney, Renewable Energy 2010 Proceedings (2010) O-Th-2-4.

[12] L. Gillan, Maisotsenko cycle for cooling processes, Int. J. Energy for a Clean Environment 9 (2008) 47–64.

[13] K.S. Ong, A mathematical model of a solar chimney, Renewable Energy 28 (2003) 1047–1060.

[14] T. Miyazaki, A. Akisawa, T. Kashiwagi, The effects of solar chimneys on thermal load mitigation of office buildings under the Japanese climate, Renewable Energy 31 (2006) 987–1010.

[15] F.P. Incropera, D.P. Dewitt, T.L. Bergman, A.S. Lavine, Fundamentals of Heat and Mass Transfer, 6th ed., Wiley, 2007.

[16] A. Hagishima, J. Tanimoto, Field measurements for estimating the convective heat transfer coefficient at building surfaces, Build. Environ. 38 (2003) 873–881.

[17] J.A. Duffie, W.A. Beckman, Solar Engineering of Thermal Processes, 2nd ed., Wiley, 1991.

[18] K.T. Andersen, Theoretical considerations on natural ventilation by thermal buoyancy, ASHRAE Trans.: Symposia SD-95-14-1 (1995) 1103–1117.

[19] American Society of Heating, Refrigerating and Air-Conditioning Engineers, ASHRAE Handbook 1985 Fundamentals, 1985.

[20] The Japan Society of Mechanical Engineers, JSME Heat Transfer Handbook (in Japanese), Maruzen, Tokyo, 1993.

[21] The Society of Heating, Air-Conditioning and Sanitary Engineers of Japan, Handbook of SHASE, Vol.3 (in Japanese), SHASE, Tokyo, 1995.

[22] K. Watanabe, Energy Efficiency Ratio for Heat Source System at Office Buildings, PhD Thesis (in Japanese), Waseda University, Tokyo, 2007.

Table 1: The radiation properties of the solar chimney materials

Property	Glass	Wall
Transmissivity	0.84	0.00
Absorptivity	0.06	0.95
Emissivity	0.9	0.9

Table 2: The materials and properties of the M-Cycle

Component	Materials	Thickness [m]	Thermal conductivity [$Wm^{-1}K^{-1}$]
Heat transfer plate	Aluminum	0.002	237
Water absorbing sheet	Fiber	0.002	0.4 (including water)
Ceiling	Plasterboard	0.01	0.5

List of Figures

Fig. 1

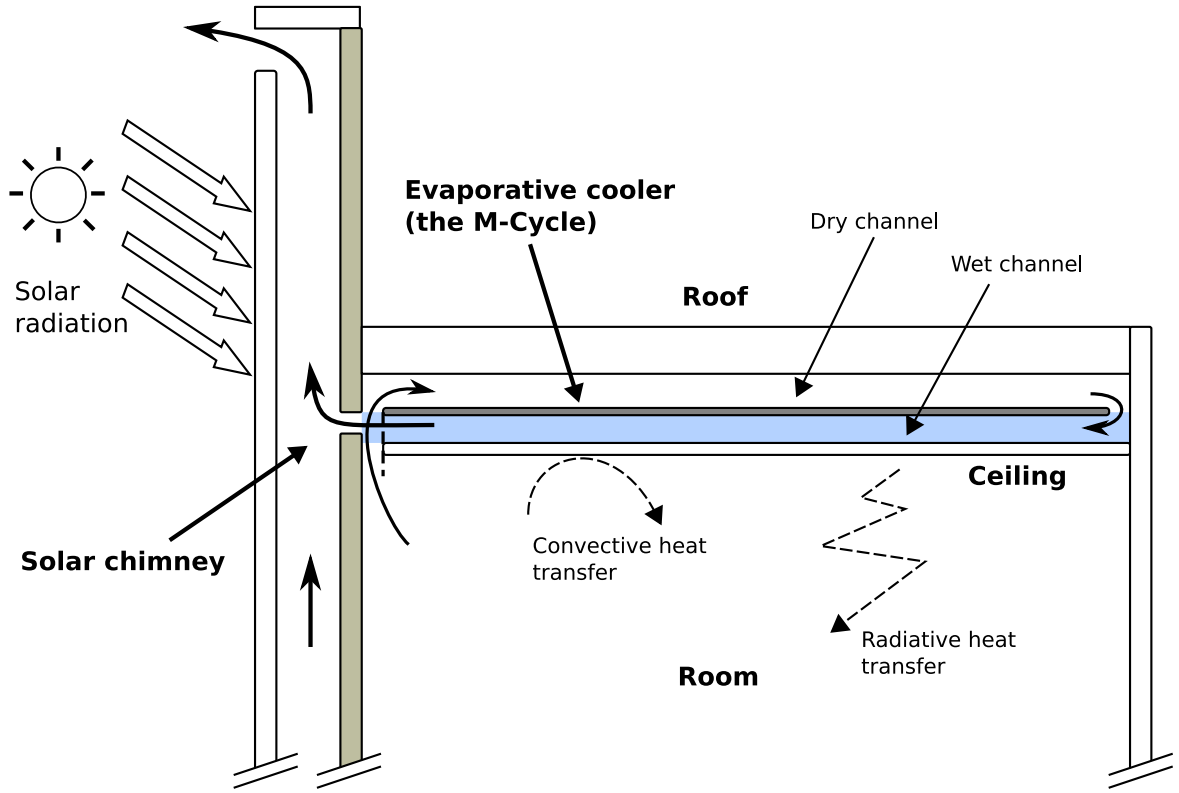
Evaporative cooler
(the M-Cycle)
Dry channel
Wet channel
Roof
Solar
radiation
Ceiling
Solar chimney
Convective heat
transfer
Radiative heat
transfer
Room

Fig. 2

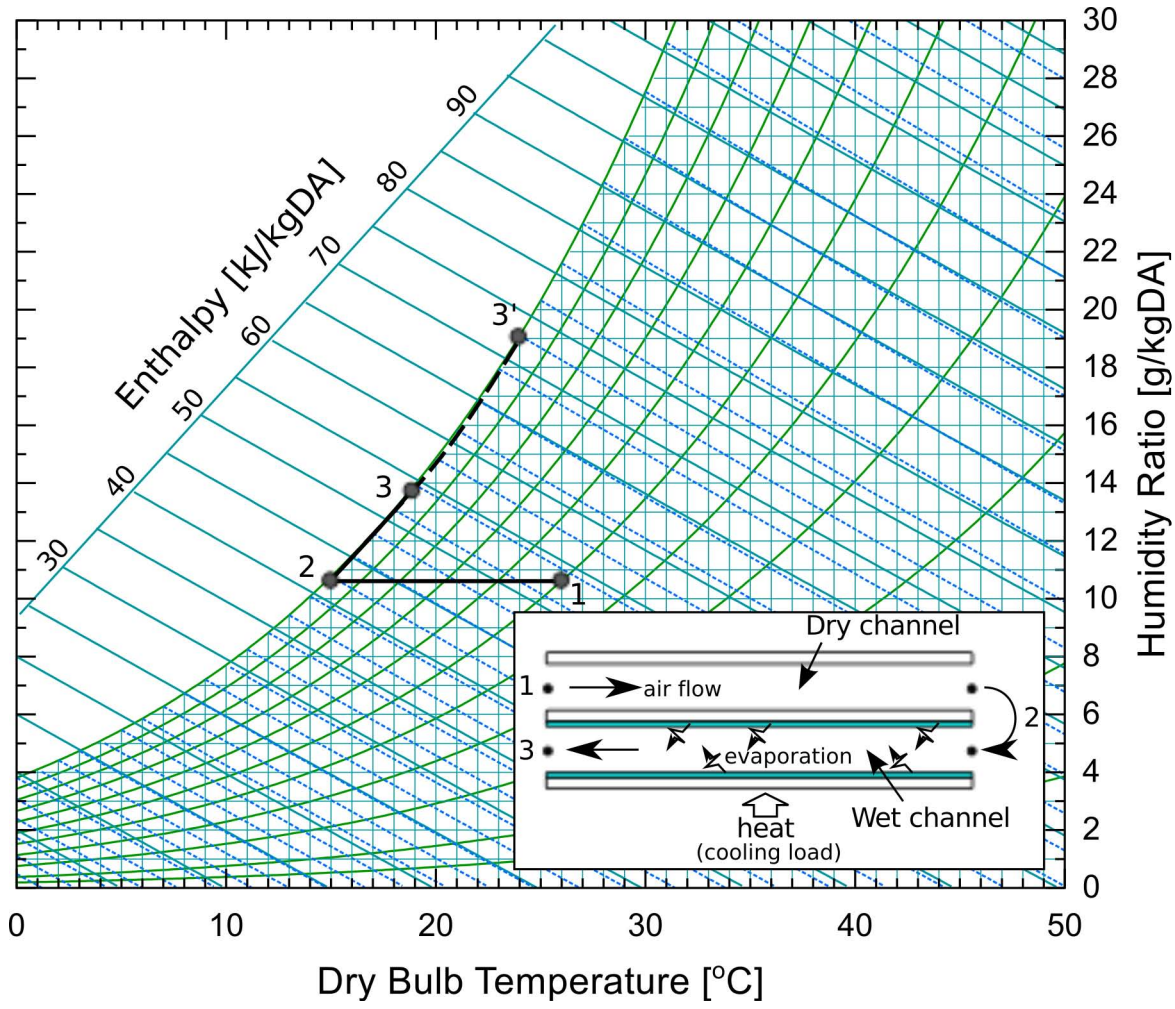
Enthalpy [kJ/kgDA]
30
40
50
60
70
80
90
Humidity Ratio [g/kgDA]
0
2
4
6
8
10
12
14
16
18
20
22
24
26
28
30
Dry Bulb Temperature [°C]
0
10
20
30
40
50
1
2
3
3'
Dry channel
air flow
evaporation
Wet channel
heat
(cooling load)

Fig. 3

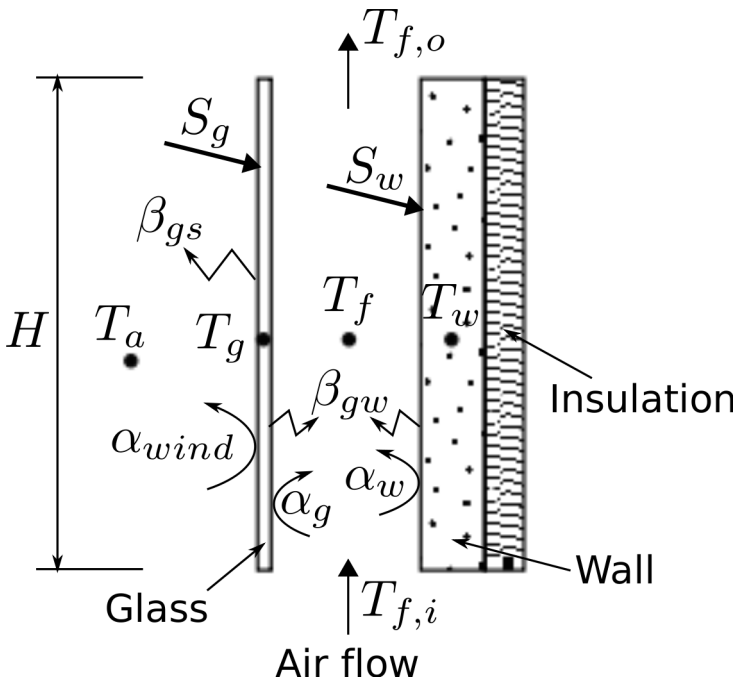
$T_{f,o}$
S_g
S_w
β_{gs}
H
T_a
T_g
T_f
T_w
Insulation
β_{gw}
α_{wind}
α_w
α_g
Wall
Glass
$T_{f,i}$
Air flow

Fig. 4

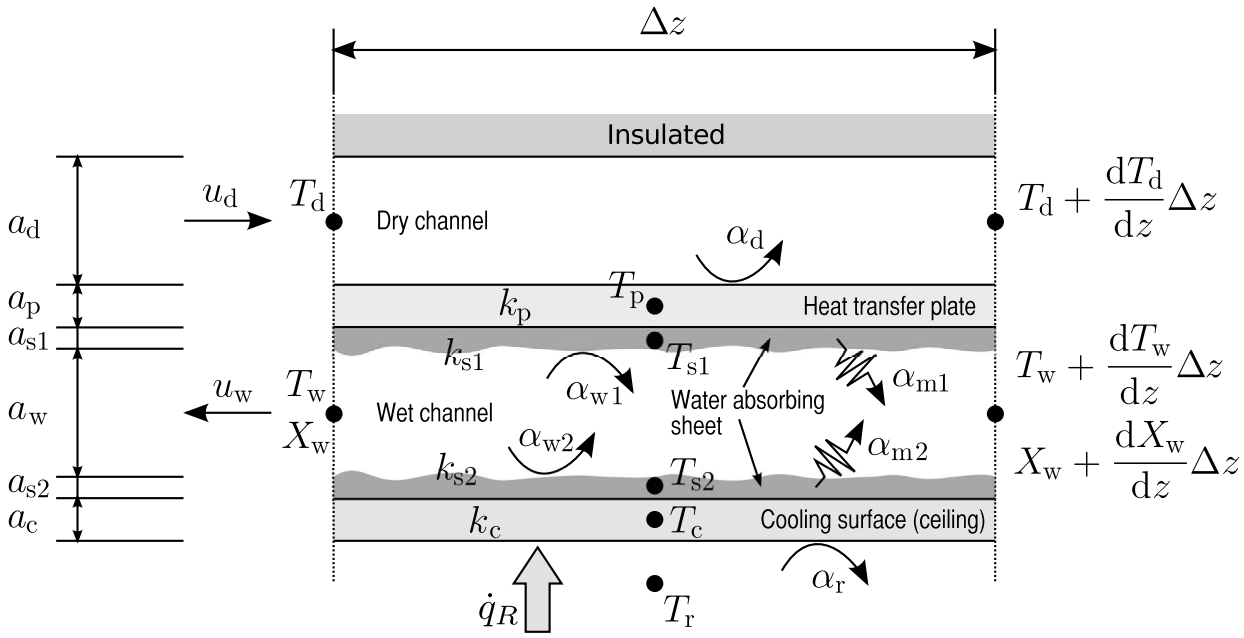
Δz
Insulated
a_{d}
a_{p}
a_{s1}
a_{w}
a_{s2}
a_{c}
u_{d}
T_{d}
Dry channel
$T_{\mathrm{d}} + \frac{\mathrm{d}T_{\mathrm{d}}}{\mathrm{d}z}\Delta z$
α_{d}
T_{p}
k_{p}
Heat transfer plate
k_{s1}
T_{s1}
α_{w1}
α_{m1}
$T_{\mathrm{w}} + \frac{\mathrm{d}T_{\mathrm{w}}}{\mathrm{d}z}\Delta z$
u_{w}
T_{w}
X_{w}
Wet channel
Water absorbing sheet
α_{w2}
α_{m2}
$X_{\mathrm{w}} + \frac{\mathrm{d}X_{\mathrm{w}}}{\mathrm{d}z}\Delta z$
k_{s2}
T_{s2}
k_{c}
T_{c}
Cooling surface (ceiling)
$\dot{q}_R$
T_{r}
α_{r}

Fig. 5

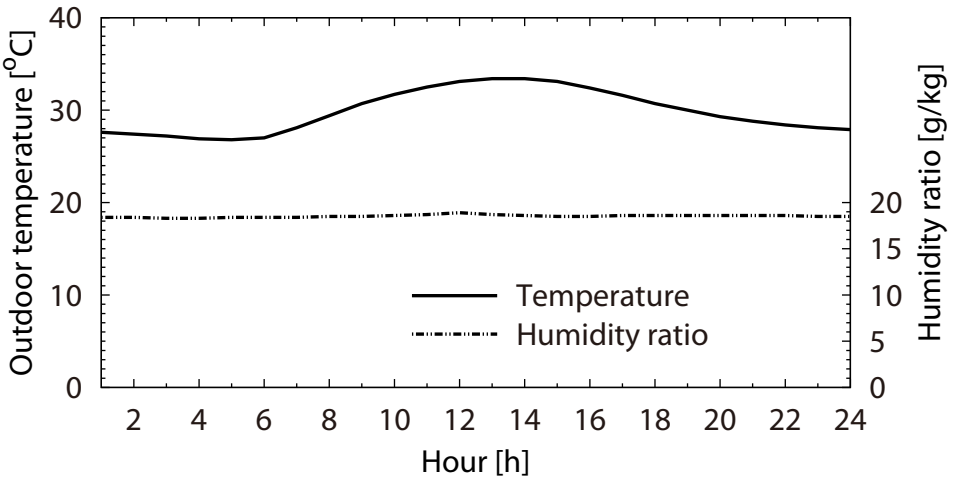
Outdoor temperature [°C]
Humidity ratio [g/kg]
Hour [h]
Temperature
Humidity ratio
0
10
20
30
40
0
5
10
15
20
2
4
6
8
10
12
14
16
18
20
22
24

Fig. 6

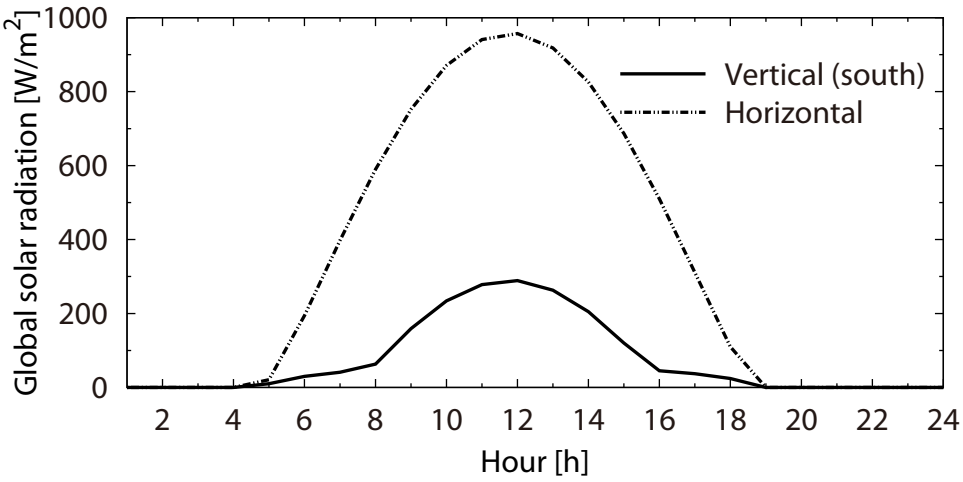
Global solar radiation [W/m2]
1000
800
600
400
200
0
2
4
6
8
10
12
14
16
18
20
22
24
Hour [h]
Vertical (south)
Horizontal

Fig. 7

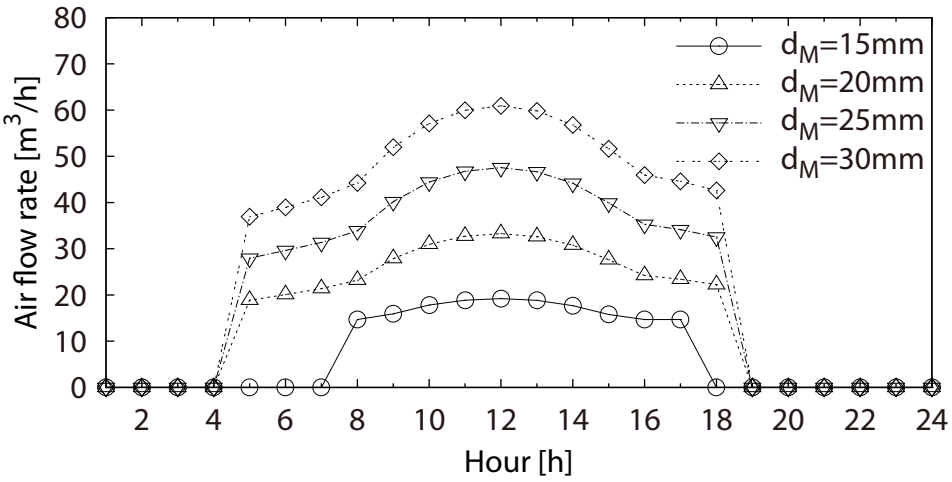
Air flow rate [m3/h]
Hour [h]
dM=15mm
dM=20mm
dM=25mm
dM=30mm
0
10
20
30
40
50
60
70
80
2
4
6
8
10
12
14
16
18
20
22
24

Fig. 8

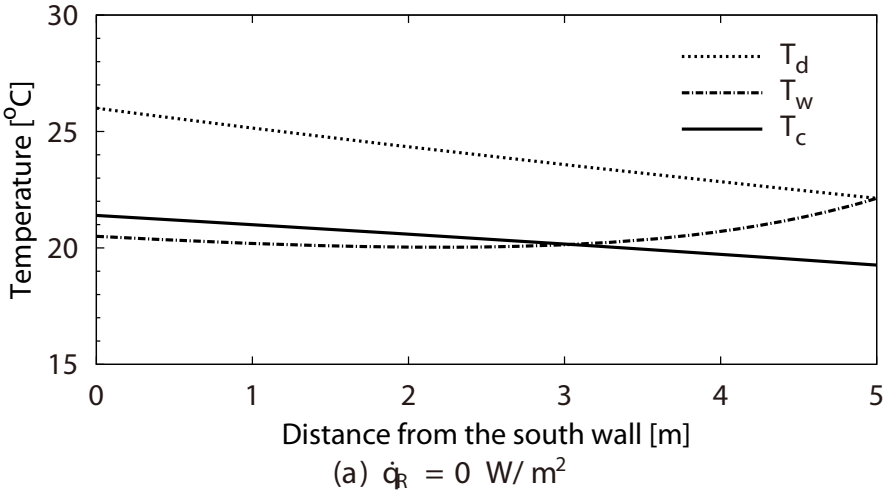

(a) $\dot{q}_R = 0$ W/ m^2

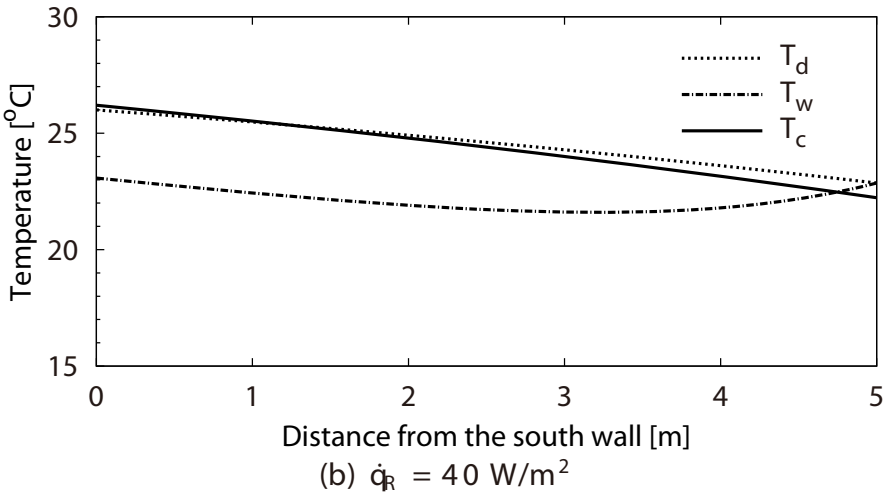

(b) $\dot{q}_R = 40$ W/m^2

Fig. 9

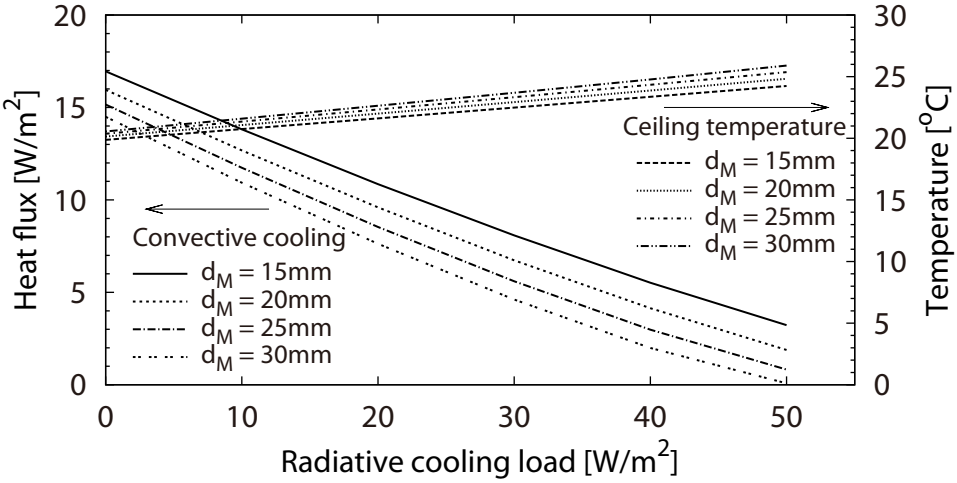
Heat flux [W/m2]
Temperature [oC]
Radiative cooling load [W/m2]
Convective cooling
dM = 15mm
dM = 20mm
dM = 25mm
dM = 30mm
Ceiling temperature
dM = 15mm
dM = 20mm
dM = 25mm
dM = 30mm
0
5
10
15
20
25
30
40
50

Fig. 10

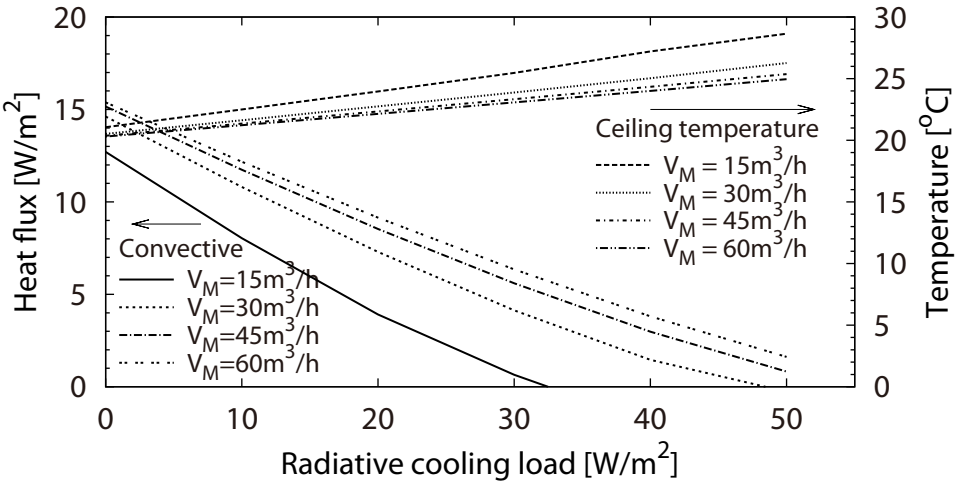
Heat flux [W/m2]
Temperature [oC]
Radiative cooling load [W/m2]
Ceiling temperature
VM = 15m3/h
VM = 30m3/h
VM = 45m3/h
VM = 60m3/h
Convective
VM=15m3/h
VM=30m3/h
VM=45m3/h
VM=60m3/h
0
5
10
15
20
25
30
40
50

Fig. 11

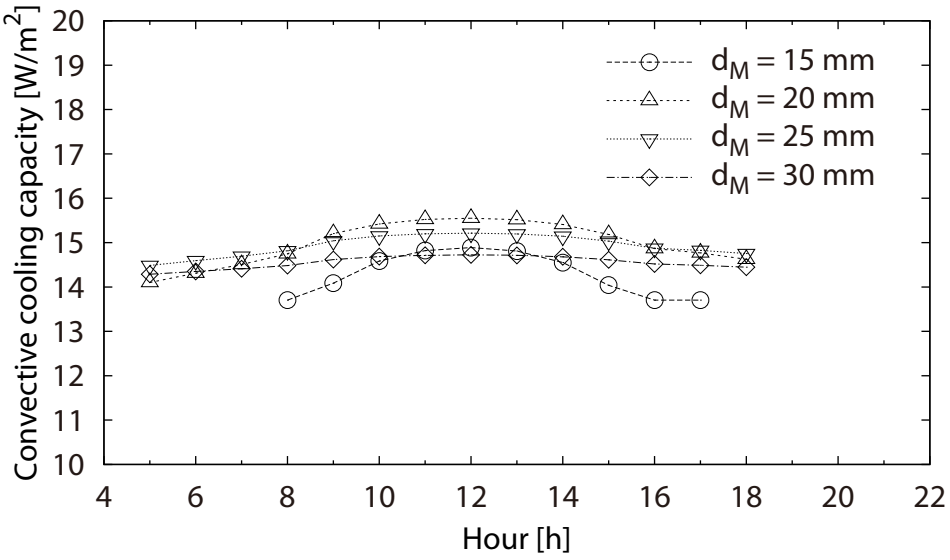
Convective cooling capacity [W/m2]
20
19
18
17
16
15
14
13
12
11
10
4
6
8
10
12
14
16
18
20
22
Hour [h]
dM = 15 mm
dM = 20 mm
dM = 25 mm
dM = 30 mm

Fig. 12

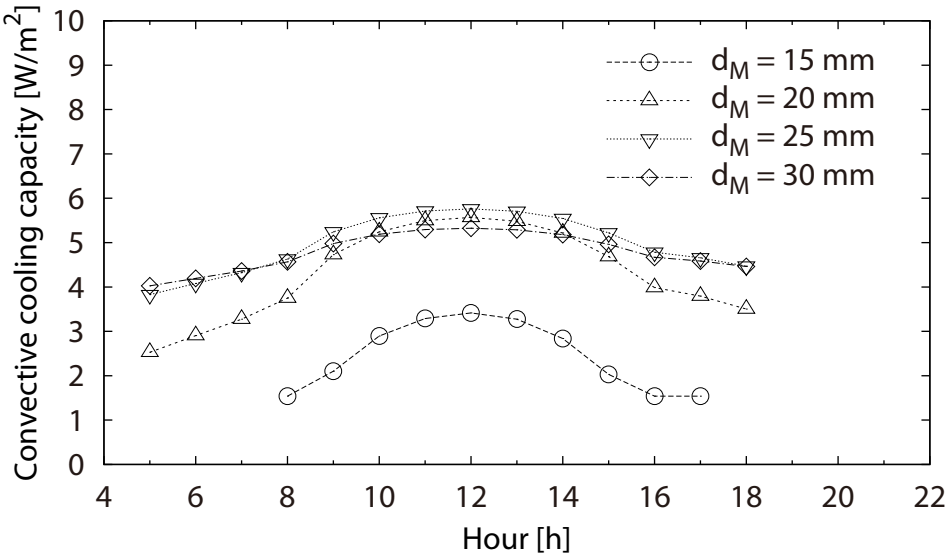
Convective cooling capacity [W/m2]
Hour [h]
dM = 15 mm
dM = 20 mm
dM = 25 mm
dM = 30 mm
0
1
2
3
4
5
6
7
8
9
10
4
6
8
10
12
14
16
18
20
22